Journal of Computational Physics 227 (2008) 8341–8366

Contents lists available at ScienceDirect

Journal of Computational Physics

journal homepage: www.elsevier.com/locate/jcp

Constructing spectral schemes of the immersed interface method via a global description of discontinuous functions

An Liang, Xiaodong Jing, Xiaofeng Sun *

School of Jet Propulsion, Beijing University of Aeronautics and Astronautics, Beijing 100083, PR China

ARTICLE INFO

Article history:
Received 31 May 2007
Received in revised form 19 March 2008
Accepted 24 May 2008
Available online 6 June 2008

Keywords:
Immersed boundary method
Immersed interface method
Spectral method
Finite difference method
Elliptic equation

ABSTRACT

A global description of discontinuous functions is introduced in this paper. By expressing a discontinuous function as the sum of a smooth function and a correction term determined by jump conditions, we turn the unknown function from a discontinuous one into a sufficiently smooth one when solving a differential equation. Spectral schemes are developed based on this concept with the intention of eliminating or reducing the Gibbs oscillation. Finite difference schemes are also constructed as an alternative of the current immersed interface methods. Both spectral and finite difference schemes are tested on one- and two-dimensional cases.

1. Introduction

There has been much research work concerning the accuracy across the boundary since Peskin first developed the immersed boundary (IB) method [4]. The original version of the IB method spreads singular sources to adjacent grids with a discrete delta function. This kind of treatment smears the jump of function value and/or its derivatives across the interface and results in first-order accuracy. In order to overcome this disadvantage, Lai and Peskin proposed a formally second-order-accurate IB method [6]. A similar scheme with formal second-order accuracy [7] was developed afterwards and applied to sufficiently smooth problems to achieve practical second-order accuracy. It is also shown in [8–10] that high-order accuracy can be achieved using the IB method for some other smooth problems. However, as addressed in literatures, the utilization of discrete delta function results in the lower order of accuracy for general cases [20,23,24].

The immersed interface method (IIM), originally developed for elliptic equations by LeVeque and Li [20], shares the same concept as the IB method by using fixed Cartesian grids and treating boundaries as singular sources but uses another approach to deal with the source term. The IIM considers the integral property of Dirac delta function and represents the effect of singular sources as a jump of function value and/or its derivatives, while the jump conditions can be derived from the source term together with the differential equation. As an example, Xu and Wang [21] shown that jump conditions of at least up to third-order spatial derivatives could be obtained for the incompressible Navier–Stokes equations. The IIM can easily achieve high-order (2nd or higher) accuracy by making modifications of standard finite difference schemes. Various finite difference schemes [20,22,23,25–29] have been constructed based on the generalized Taylor expansion, which takes discontinuities into account, or through the matched polynomial interpolation. The IIM has also been incorporated with the finite volume method [31] and the finite element method [30].

* Corresponding author. Tel./fax: +86 10 82317408.
E-mail address: sunxf@buaa.edu.cn (X. Sun).

0021-9991/$ - see front matter © 2008 Elsevier Inc. All rights reserved.
doi:10.1016/j.jcp.2008.05.020

The IB and IIM have been widely applied to flow field simulations including cardiovascular physiology [4,12], swimming aquatic animals [13,14], multiphase flows [15,16,24], engine modeling [17,18], aerodynamic problems [5,6,11,19] and so forth. In the field of computational fluid dynamics, the spectral methods have been attracting persistent research interests for some extraordinary advantages [1–3,32–35]. However, the application areas of spectral methods are limited due to the strict requirement of the simplicity of computational domain and the smoothness of the solution. The IB/IIM simplifies the computational domain to regular geometries such as rectangles in two-dimensional cases and cuboids in three-dimensional cases but, at the same time, brings unsmoothness or even discontinuity across the boundaries immersed in the fluid. There have been some efforts to incorporate the IB method to the spectral methods [5,38] but the overshooting phenomenon and spatial oscillations, known as the Gibbs phenomenon, remains unsolved. Some other authors [39–41] endeavored to use spectral methods with volume-penalization, a method similar to the IB method in concept, in flow field simulations and encountered the Gibbs phenomenon as well. The effects of the Gibbs phenomenon in these methods are discussed in [11,38–41].

To the authors' knowledge, all current IIM methods are based on the local modification of schemes near the interfaces and little effort has been made to incorporate the IIM with the spectral methods without incurring Gibbs phenomenon. In this paper, a global description of discontinuous functions is proposed. In our global description, a discontinuous function is represented as the sum of a smooth function and a correction term only related to jump conditions. This concept turns the unknown function from a discontinuous function into another smooth function. Thus, the spectral method is possible to be applied and an alterative approach to construct finite difference schemes is also provided. Although aiming at the simulation of fluid flow problems, as a preliminary step, the present paper discusses only the elliptic equations just as LeVeque and Li [20] and Zhong [23] did previously.

In this paper, we first introduce our concept for one-dimensional cases as well as finite difference and spectral implementation in Section 2. An extension from one-dimensional to higher dimensional cases is presented in Section 3 with an example. Section 4 gives the conclusion.

2. One-dimensional cases

2.1. Basic formulation

We begin by introducing a global description of a piecewise smooth function in one-dimensional case. Suppose $u(x)$ is a piecewise smooth function on the interval $[a,b]$ with a finite jump of function value and/or its derivatives at position $x=\alpha$. Thus $u(x)$ can be expressed in a traditional way as:

$$u(x)=\begin{cases} f(x), & x\in[a,\alpha] \\ g(x), & x\in[\alpha,b] \end{cases} \tag{1}$$

where $f(x)$ and $g(x)$ are C^∞ functions in their domain of definition. A global description of $u(x)$ for this case is proposed here as

$$u(x)=f(x)+H(x-\alpha)[g(x)-f(x)] \tag{2}$$

by introducing the unit step function $H(x)$, also referred as the Heaviside function, which is defined as

$$H(t)=\begin{cases} 0, & t<0 \\ 1, & t>0 \end{cases} \tag{3}$$

It should be noticed that the domain of definition of $f(x)$ is extended from $[a,\alpha]$ to $[a,b]$ and the function value of $f(x)$ on the interval $[\alpha,b]$ is not determined. Thus the term $g(x)-f(x)$ is not unique but depends on how we construct a C^∞ extension of $f(x)$. For a more general case with m discontinuous points, (2) reads

$$u(x)=u_c(x)+\sum_{j=1}^{m}H(x-\alpha_j)p_j(x) \tag{4}$$

where $u_c(x)$ and $p_j(x)$ are C^∞ functions and the symbol α_j denotes the jth discontinuous point. It will be shown below that functions $p_j(x)$ must satisfy certain conditions to ensure the smoothness of $u_c(x)$ although they are not determined and are left to be constructed. Taking derivative of (4) with respect to x, we obtain

$$u'=u_c'+\sum_{j=1}^{m}[H(x-\alpha_j)p_j'(x)+p_j\delta(x-\alpha_j)] \tag{5}$$

where $\delta(x)$ denotes the Dirac delta function. Noticing that $\delta(x)$ vanishes when $x\neq 0$, we obtain the expression of the first-order derivative of $u(x)$ at continuous points

$$u'(x)=u_c'(x)+\sum_{j=1}^{m}[H(x-\alpha_j)p_j'(x)],\quad x\neq\alpha_j \tag{6}$$

When x coincides with one of the discontinuous point α_l, by integrating (5) from α_{l-} to α_{l+} we obtain

$$\begin{aligned}[u]|_{\alpha_l} &= \int_{\alpha_{l-}}^{\alpha_{l+}} u'(x)\mathrm{d}x \\ &= \int_{\alpha_{l-}}^{\alpha_{l+}} u_c'(x)\mathrm{d}x + \sum_{j=1}^{m}\left[\int_{\alpha_{l-}}^{\alpha_{l+}} H(x-\alpha_j)p_j'(x)\mathrm{d}x + \int_{\alpha_{l-}}^{\alpha_{l+}} p_j\delta(x-\alpha_j)\mathrm{d}x\right] \\ &= p_l(\alpha_l)\end{aligned} \tag{7}$$

where $[u]|_{\alpha_l} = u(\alpha_{l+}) - u(\alpha_{l-})$ denotes a jump of function $u(x)$ at $x = \alpha_l$. Similarly, the nth order derivative of $u(x)$ can be obtained as

$$u^{(n)} = u_c^{(n)} + \sum_{j=1}^{m}[H(x-\alpha_j)p_j^{(n)}(x)], \quad x \neq \alpha_j \tag{8}$$

$$[u^{(n)}]|_{\alpha_j} = p_j^{(n)}(\alpha_j) \tag{9}$$

Eq. (9) is the constraint for constructing $p_j(x)$. It can also be obtained by simply considering the difference between the right and the left limit of $u^{(n)}$ at discontinuous points. It can also be proved that when substituting $x = \alpha_j$ into (8), we obtain $u^{(n)}(\alpha_{j-})$ if we define $H(0) = 0$ and $u^{(n)}(\alpha_{j+})$ if $H(0) = 1$. Thus we can still use (8) in numerical computation without encountering any singularity when the point coincides with one of the discontinuous points.

It should be addressed that a similar idea was introduced by Abarbanel et al. [42] to extract information form an oscillatory solution by spectral methods for discontinuous problem, where a saw-tooth function was used as the "correction function".

2.2. Finite difference and spectral collocation schemes

The function $u(x)$ in (4) is usually assumed to be the solution of a differential equation with singular sources. Our strategy for solving such differential equation is to construct $p_j(x)$ which satisfies the jump conditions (9) and then correct the approximation of the derivatives of $u(x)$. A detailed formulation is discussed below.

Let the vectors $\mathbf{U^{(n)}}$, $\mathbf{P^{(n)}}$ and $\mathbf{U_c^{(n)}}$ represent the value of nth order derivative ($n \geqslant 0$) of function $u(x)$, $\sum_{j=1}^{m}[H(x-\alpha_j)p_j^{(n)}(x)]$ and $u_c(x)$, respectively at $x = x_0, x_1, \ldots, x_N$, the discrete points in finite difference method or collocation points in the spectral collocation method. According to (8), it is clear that

$$\mathbf{U^{(n)}} = \mathbf{U_c^{(n)}} + \mathbf{P^{(n)}} \tag{10}$$

Since $u_c(x)$ is a C^∞ function, $\mathbf{U_c^{(n)}}$ can be computed from $\mathbf{U_c} = \mathbf{U_c^{(0)}}$ in both finite difference method and spectral collocation method by introducing the nth order derivative matrix $\mathbf{D^{(n)}}$:

$$\mathbf{U_c^{(n)}} = \mathbf{D^{(n)}U_c} \tag{11}$$

Substituting (11) into (10) yields

$$\begin{aligned}\mathbf{U^{(n)}} &= \mathbf{D^{(n)}U_c} + \mathbf{P^{(n)}} \\ &= \mathbf{D^{(n)}U} - \mathbf{D^{(n)}P} + \mathbf{P^{(n)}}\end{aligned} \tag{12}$$

Eq. (12) gives the approximation of derivatives of a discontinuous function $u(x)$ using its values at discrete point set. It is noticeable that no modification is made to the derivative matrix and the correction terms ($-\mathbf{D^{(n)}P} + \mathbf{P^{(n)}}$) at the right hand side can be calculated explicitly. Theoretically, the order of accuracy depends only on the order of accuracy of the derivative matrix, but in most conditions, only lower order jump conditions are available for us to construct the correction function $p_j(x)$ and that may result in a reduction in the order of accuracy. However, a second- or fourth-order-accurate scheme is usually acceptable for most practical applications.

2.3. Galerkin type method

A direct expansion of the discontinuous function $u(x)$ in Eq. (4) and its derivatives is expected to incur overshoot phenomenon near the discontinuous points and excite oscillation all over the whole computational domain, which is known as the Gibbs phenomenon, so we consider the C^∞ function $u_c(x)$ instead. The nth order ($n \geqslant 0$) derivative of $u_c(x)$ is approximated by a truncated series as:

$$u_c^{(n)}(x) \doteq u_{cN}^{(n)}(x) = \sum_{k=0}^{N}\hat{v}_k^{(n)}\varphi_k(x) \tag{13}$$

where the basis functions are denoted as $\varphi_k(x)$. The coefficient $\hat{v}_k^{(n)}$ for each basis function $\varphi_k(x)$ can be determined by

$$\hat{v}_k^{(n)} = \frac{1}{c_k}\int_a^b u_c^{(n)}\varphi_k w\mathrm{d}x \tag{14}$$

if the basis functions are orthogonal with respect to some weight $w(x)$, i.e.

$$\int_a^b \varphi_k \varphi_l w \mathrm{d}x = c_k \delta_{k,l} \tag{15}$$

where c_k = const. and $\delta_{k,l}$ is the Kronecker delta. Thus we obtain an alterative expansion of the discontinuous $u(x)$ and its derivatives as

$$u^{(n)}(x) \doteq u_N^{(n)}(x) = \sum_{k=0}^{N} \hat{v}_k^{(n)} \varphi_k + \sum_{j=1}^{m} H(x-\alpha_j) p_j^{(n)}(x) \tag{16}$$

which removes the Gibbs phenomenon. We define the following vectors

$$\widehat{\mathbf{V}}^{(\mathbf{n})} = (\hat{v}_0^{(n)}, \hat{v}_1^{(n)}, \ldots, \hat{v}_N^{(n)})^{\mathbf{T}} \tag{17}$$

then, similar to the finite difference method and the spectral collocation method, an nth order derivative matrix $\widehat{\mathbf{D}}^{(\mathbf{n})}$ can be found so that

$$\widehat{\mathbf{V}}^{(\mathbf{n})} = \widehat{\mathbf{D}}^{(\mathbf{n})} \widehat{\mathbf{V}} \tag{18}$$

It should be noticed that appliance of the weighted residual method to (16) induces the following integration term

$$\int_a^b \left\{ \sum_{j=1}^{m} H(x-\alpha_j) p_j^{(n)}(x) \right\} \varphi_i(x) \mathrm{d}x$$

For the sake of simplicity, we define

$$\widehat{\mathbf{P}}^{(\mathbf{n})} = \begin{pmatrix} \int_a^b \left\{ \sum_{j=1}^{m} H(x-\alpha_j) p_j^{(n)}(x) \right\} \varphi_0(x) \mathrm{d}x \\ \int_a^b \left\{ \sum_{j=1}^{m} H(x-\alpha_j) p_j^{(n)}(x) \right\} \varphi_1(x) \mathrm{d}x \\ \vdots \\ \int_a^b \left\{ \sum_{j=1}^{m} H(x-\alpha_j) p_j^{(n)}(x) \right\} \varphi_N(x) \mathrm{d}x \end{pmatrix} \tag{19}$$

Since the correction functions $p_j(x)$ are known beforehand, $\widehat{\mathbf{P}}^{(\mathbf{n})}$ defined in (19) are known vectors. We then give another form of (19) which is more appropriate for numerical calculation. The order of integration and summation symbol in (19) can be exchanged, i.e.

$$\widehat{\mathbf{P}}^{(\mathbf{n})} = \begin{pmatrix} \sum_{j=1}^{m} \left\{ \int_a^b H(x-\alpha_j) p_j^{(n)}(x) \varphi_0(x) \mathrm{d}x \right\} \\ \sum_{j=1}^{m} \left\{ \int_a^b H(x-\alpha_j) p_j^{(n)}(x) \varphi_1(x) \mathrm{d}x \right\} \\ \vdots \\ \sum_{j=1}^{m} \left\{ \int_a^b H(x-\alpha_j) p_j^{(n)}(x) \varphi_N(x) \mathrm{d}x \right\} \end{pmatrix} \tag{20}$$

Noticing each integrand vanishes when $x < \alpha_j$, we eliminate the Heaviside functions by adjusting the range of integration. Thus (19) reads

$$\widehat{\mathbf{P}}^{(\mathbf{n})} = \begin{pmatrix} \sum_{j=1}^{m} \left\{ \int_{\alpha_j}^b p_j^{(n)}(x) \varphi_0(x) \mathrm{d}x \right\} \\ \sum_{j=1}^{m} \left\{ \int_{\alpha_j}^b p_j^{(n)}(x) \varphi_1(x) \mathrm{d}x \right\} \\ \vdots \\ \sum_{j=1}^{m} \left\{ \int_{\alpha_j}^b p_j^{(n)}(x) \varphi_N(x) \mathrm{d}x \right\} \end{pmatrix} \tag{21}$$

Then the integration can be evaluated either analytically or through a numerical quadrature.

2.4. Formation of the correction function $p_j(x)$

The correction function $p_j(x)$ is expected to satisfy all the jump conditions at the corresponding discontinuous point $x = \alpha_j$. However, only jump conditions for the lower order derivatives can be acquired for most differential equation(s). In this case, $p_j(x)$ can be constructed as a polynomial. More precisely, if up to lth order jump conditions are known at $x = \alpha_j$, the corresponding $p_j(x)$ can be constructed as

$$p_j(x) = \sum_{k=0}^{l} \frac{[u^{(k)}]}{k!}(x-\alpha_j)^k \tag{22}$$

It is assumed implicitly in (22) that higher order derivative jumps are equal to zero.

It should be noted that polynomial is not the only choice. As will be shown in the next section, an exponential form of $p_j(x)$ is chosen to satisfy all the jump conditions for a special case.

2.5. An example for one-dimensional boundary value problems

Solution of a second-order ordinary differential equation with Dirichlet boundary conditions

$$\begin{cases} u'' - u' = \delta(x) & \text{on} \quad (-1,1) \\ u(-1) = u(1) = 0 \end{cases} \tag{23}$$

using the finite difference/spectral collocation scheme (12) and Galerkin method is introduced in this section. The first two jump conditions are easily acquired as

$$\begin{aligned} [u]|_0 &= 0 \\ [u^{(1)}]|_0 &= 1 \end{aligned} \tag{24}$$

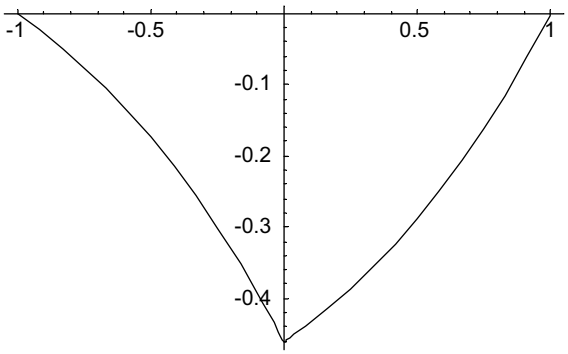

Fig. 1. Exact solution of differential Eq. (23).

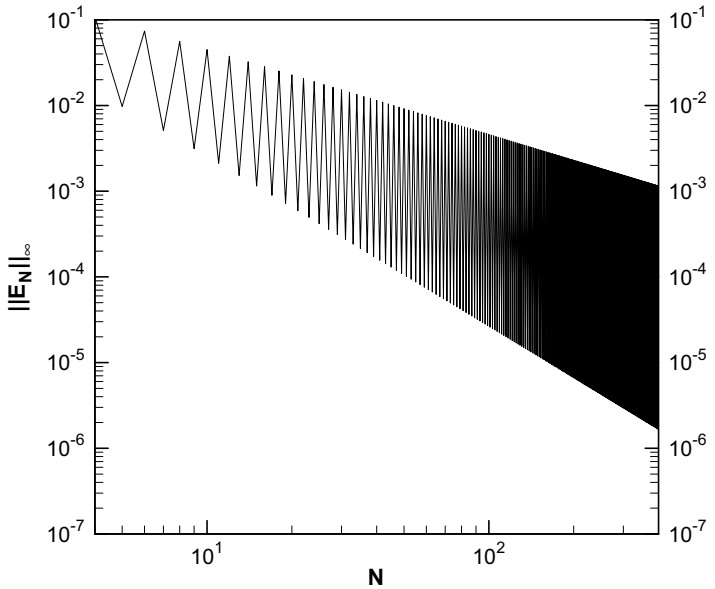

Fig. 2. Error of finite difference method for the 1D example with 1st order jump condition.

At $x = 0^+$ and $x = 0^-$, (23) reads

$$u'' = u' \tag{25}$$

The relation

$$u^{(n)} = u^{(n-1)} \tag{26}$$

at $x = 0^+$ and $x = 0^-$ can be obtained by differentiating (25) with respect to x. Thus the jump condition for the present problem is

$$\begin{aligned} &[u]|_0 = 0 \\ &[u^{(n)}]|_0 = 1, \quad n \geqslant 1 \end{aligned} \tag{27}$$

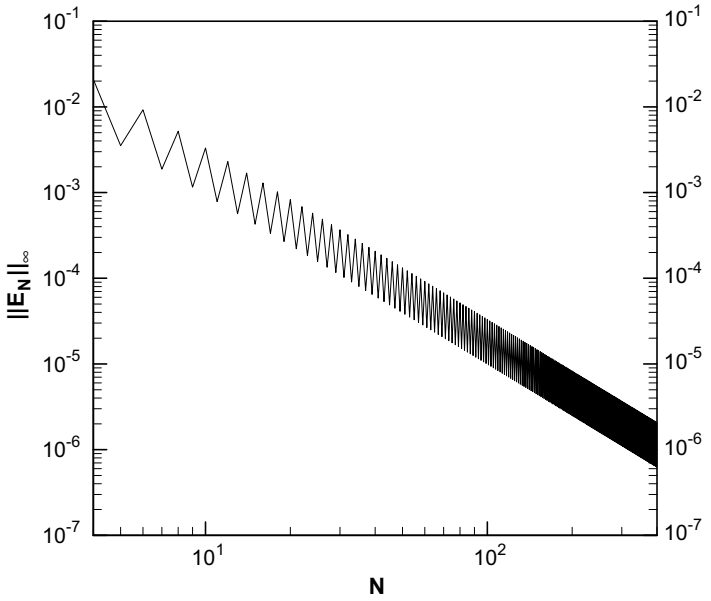

Fig. 3. Error of finite difference method for the 1D example with 2nd order jump condition.

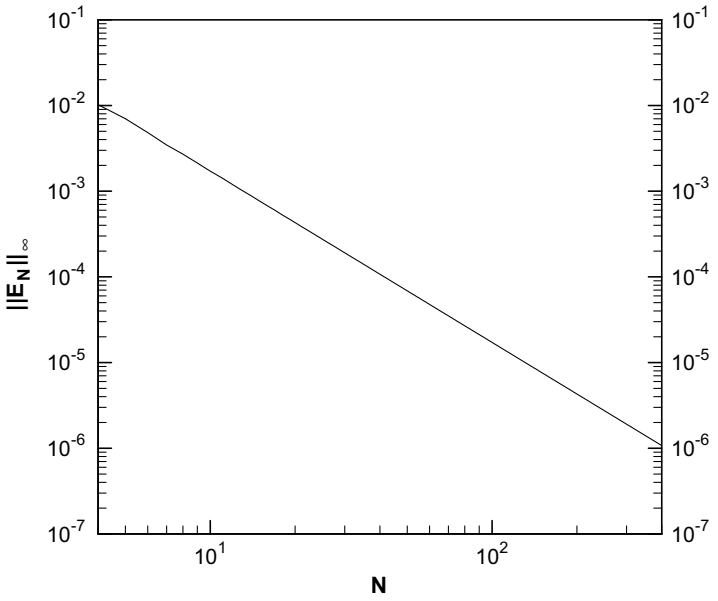

Fig. 4. Error of finite difference method for the 1D example with 3rd order jump condition.

The exact solution of (23) is

$$u = -\frac{e}{1+e}e^x + (e^x - 1)H(x) + \frac{1}{1+e} \tag{28}$$

and the plot is shown in Fig. 1.

2.6. Finite difference and spectral collocation method

The finite difference/spectral collocation scheme for this problem is

$$(\mathbf{D}^{(2)} - \mathbf{D})\mathbf{U} = \mathbf{D}^{(2)}\mathbf{P} - \mathbf{P}^{(2)} - \mathbf{D}\mathbf{P} + \mathbf{P}^{(1)} \tag{29}$$

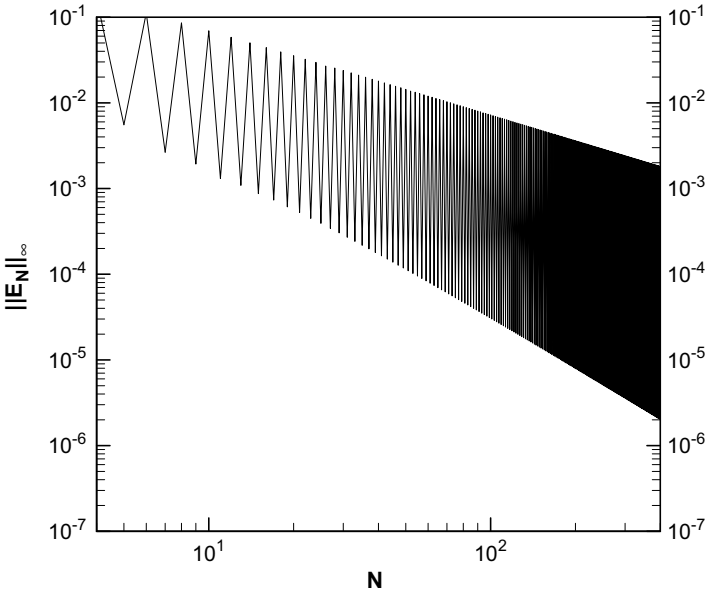

Fig. 5. Error of the Chebyshev collocation method for the 1D example with 1st order jump condition.

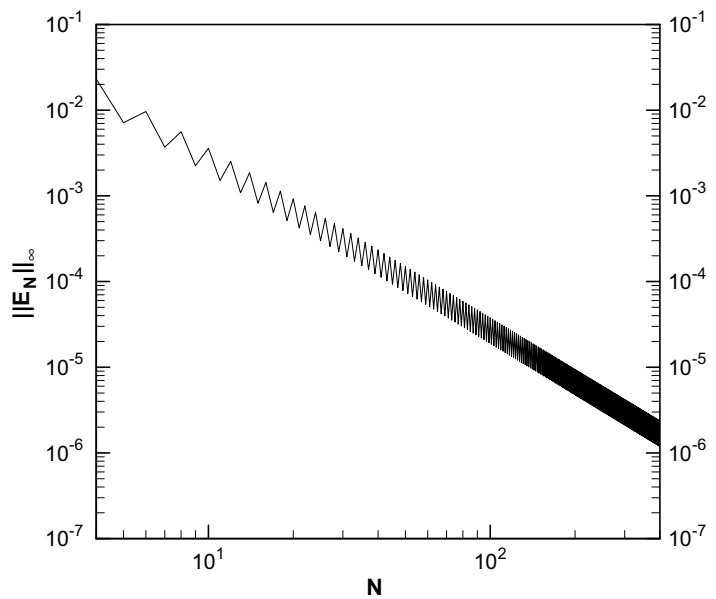

Fig. 6. Error of the Chebyshev collocation method for the 1D example with 2nd order jump condition.

while the first and last row of the coefficient matrix and the right hand side vector are replaced to represent the boundary condition. A standard 3-points central finite difference scheme with uniform grid and the Chebyshev collocation method with Gauss-Lobatto points were used for Eq. (29). The calculation of derivative matrices for the Chebyshev collocation method can be found in [3]. In Figs. 2–7, the maximum error over all grid points

$$\|E_N\|_\infty = \max_i |u(x_i) - u_i| \tag{30}$$

where u_i is the computed approximation at the grid point x_i and $u(x_i)$ is the exact solution, is plotted against the number of grid points N in log scales, with different orders of jump conditions l, which indicates that jump conditions from $[u]$ to $[u^{(l)}]$ are given. In this section, the order of jump conditions l is adjusted by constructing an l-degree polynomial as correction function using (22). Numerical results and the exact solution are compared in Figs. 8–13 with the configurations of $N = 40$, $l = 1$–3. The spatial distributions of error are also plotted for those configurations in Figs. 14–17. It can be observed

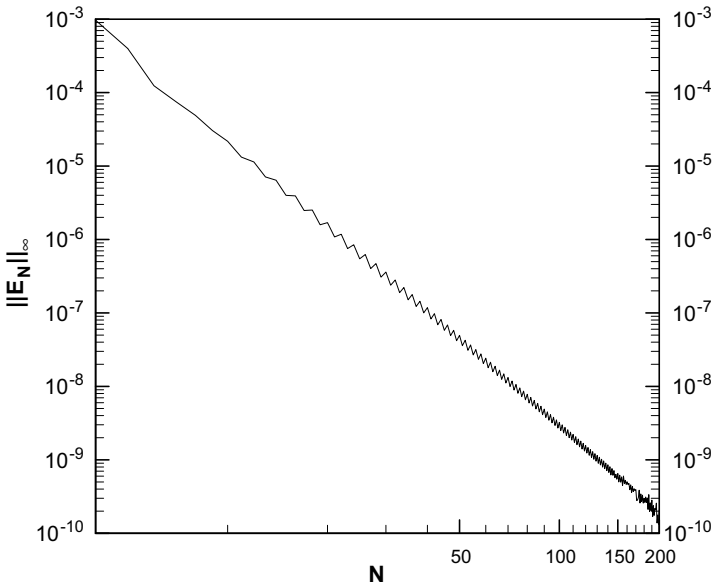

Fig. 7. Error of the Chebyshev collocation method for the 1D example with 3rd order jump condition.

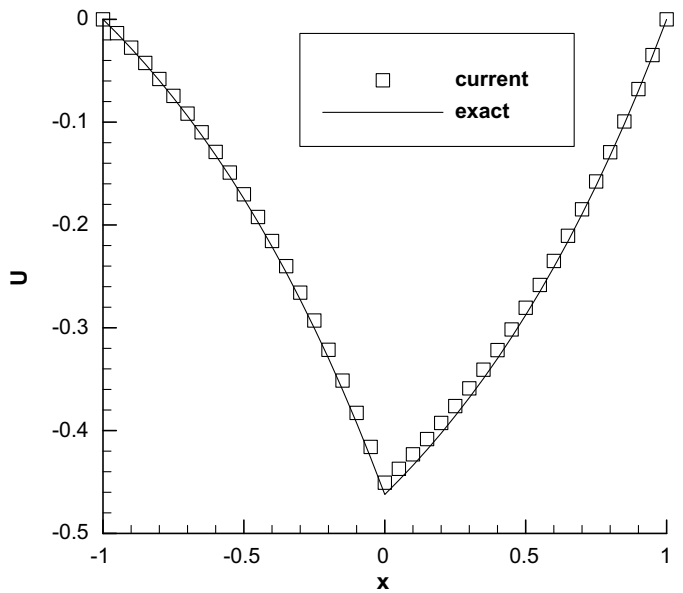

Fig. 8. Numerical solution for the 1D example using finite difference method with $N = 40$, $l = 1$.

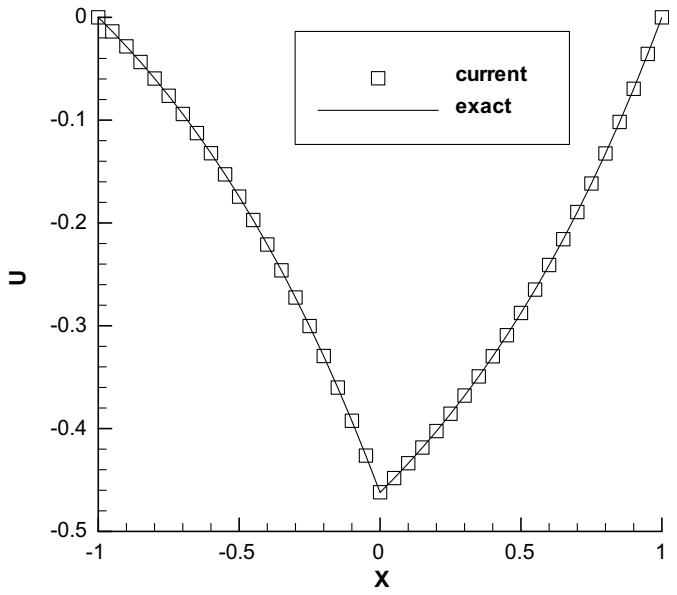

Fig. 9. Numerical solution for the 1D example using finite difference method with $N = 40$, $l = 2$.

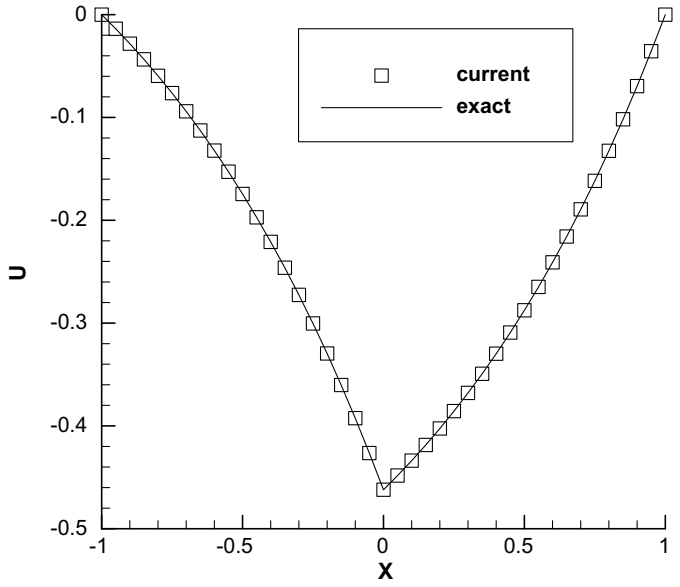

Fig. 10. Numerical solution for the 1D example using finite difference method with $N = 40$, $l = 3$.

from the above numerical results that the sharp interface is successfully simulated and there is no sign of Gibbs oscillations. It is implied in some papers that Gibbs oscillation is much more severe if the solution is discontinuous, i.e. with a jump in function value, and the oscillation can be greatly suppressed even if only the 0th order jump condition is satisfied. As an example, Abarbanel et al. [42] developed a method to extract information form an oscillatory solution of spectral methods for discontinuous problem. The concept of that procedure is to find a smooth function and a saw-tooth function (with unknown jump at an unknown location), the summation of which makes up the solution. Although this method is expected to satisfy only the 0th order jump condition for general cases, the result represents the piecewise smooth solution rather well.

We then attempt to give a brief explanation of the error oscillations observed in Figs. 2,3,5 and 6 as follows. It can be proved that the finite difference version of (12) can also be obtained using the generalized Taylor expansion referred in [22]

$$g(z_{m+1}^-) = \sum_{n=0}^{\infty} \frac{g^{(n)}(z_0^+)}{n!}(z_{m+1} - z_0)^n + \sum_{l=1}^{m} \sum_{n=0}^{\infty} \frac{[g^{(n)}(z_l)]}{n!}(z_{m+1} - z_l)^n \tag{31}$$

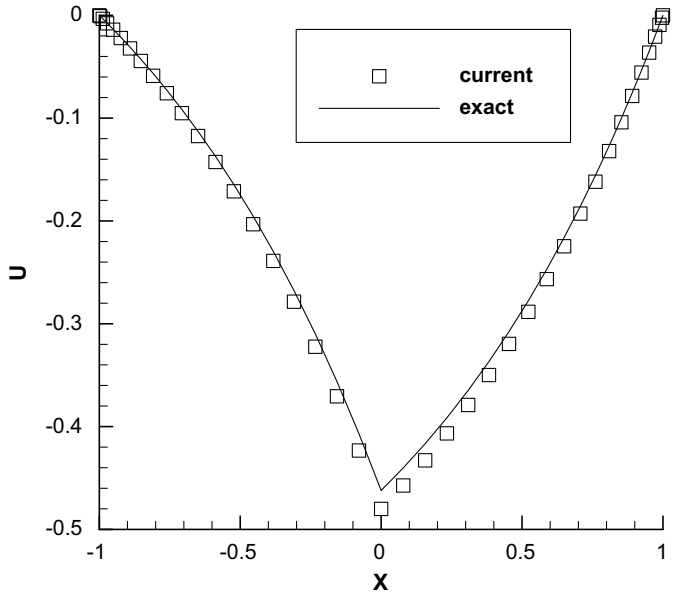

Fig. 11. Numerical solution for the 1D example using Chebyshev collocation method with $N = 40$, $l = 1$.

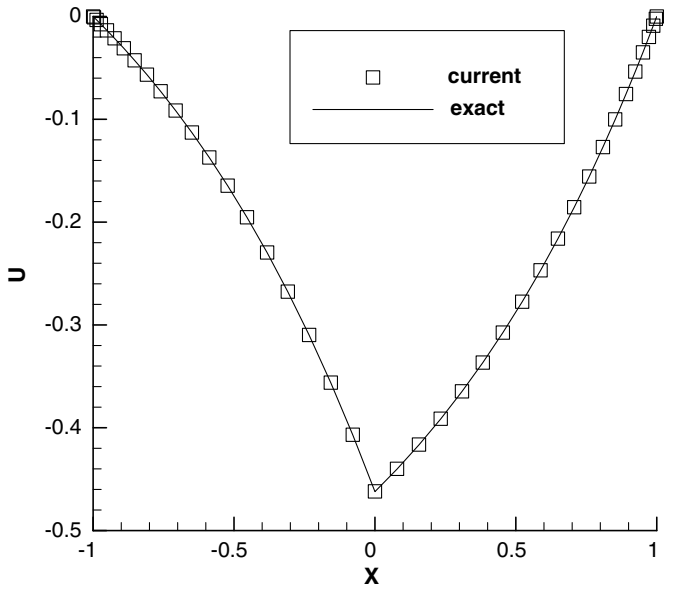

Fig. 12. Numerical solution for the 1D example using Chebyshev collocation method with $N = 40$, $l = 2$.

Specially, our scheme is equivalent to LeVeque and Li's scheme [20] with 1st order jump condition and a corresponding 1-degree polynomial correction function. The term $(z_{m+1} - z_l)$ in (31), i.e. the distance between the irregular point z_{m+1} and the discontinuous point z_l does not monotonically decrease with the increase of N, which causes the error oscillation for our finite difference schemes. The Chebyshev collocation method can be understood as a high-order interpolation method, and thus the explanation above is also applicable for our Chebyshev collocation schemes. However, it must be addressed that the error oscillation does not seem to be the necessary consequence of the current global description concept, as will be evidenced by our numerical results from Chebyshev-tau method later.

We define the order r for each scheme by applying a power fit to the error data, i.e.

$$\|E_N\|_\infty = \text{const.} \cdot N^{-r} \tag{32}$$

using least square method. The calculated orders for the above schemes are listed in Table 1. It is seen from the figures and Table 1 that the order for the finite difference scheme is determined by the order of derivative matrices together with the

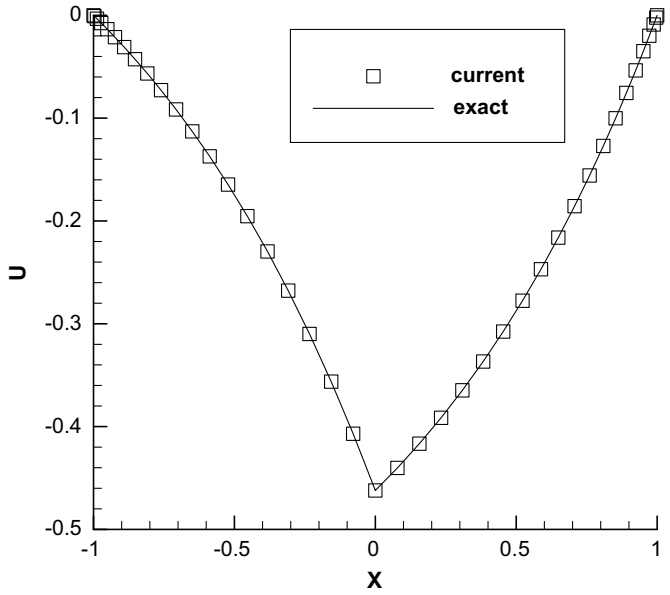

Fig. 13. Numerical solution for the 1D example using Chebyshev collocation method with $N = 40$, $l = 3$.

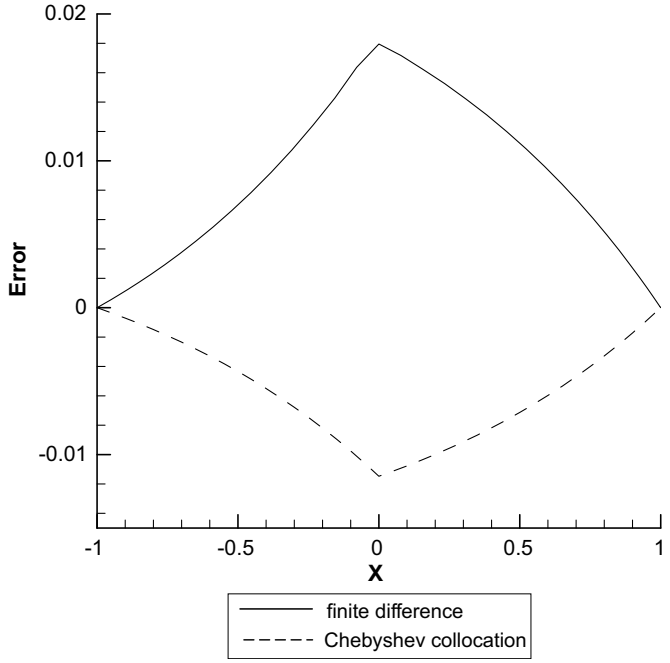

Fig. 14. Error distribution with $N = 40$, $l = 1$.

order of jump condition. As for the spectral method, the error is proportional to $\frac{1}{N^N}$ for smooth problems, so the order is restricted by the order of jump condition. We can construct the correction function as

$$p_1 = e^x - 1 \tag{33}$$

to satisfy all the jump conditions given in (27), thus the Chebyshev collocation scheme recovers the spectral accuracy as shown in Fig. 18, where the oscillation of error at $N > 12$ is believed to be caused by round-off errors.

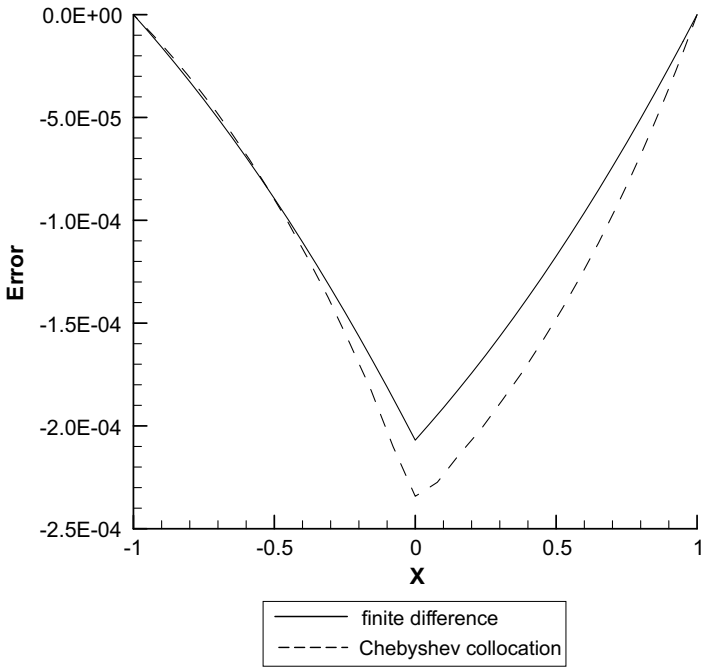

Fig. 15. Error distribution with $N = 40$, $l = 2$.

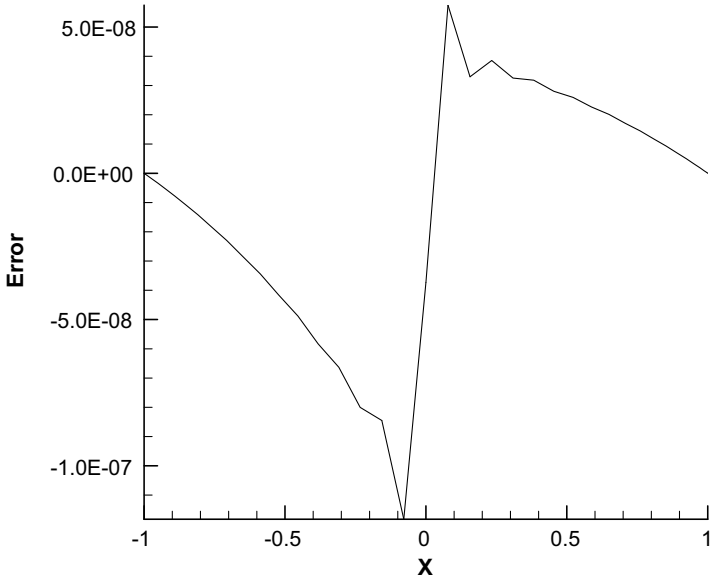

Fig. 16. Error distribution with $N = 40$, $l = 3$, Chebyshev collocation method.

2.7. Galerkin type method

It is assumed that solution of differential Eq. (23) has the following form:

$$u = \sum_{k=0}^{N} \hat{u}_k T_k(x) + H(x)p_1(x) \tag{34}$$

where $T_k(x)$ is the kth degree Chebyshev polynomial and p_1 is the correction function either in polynomial form (22) or in exponential function form (33). Application of Galerkin weighted residual method in this problem yields the linear system

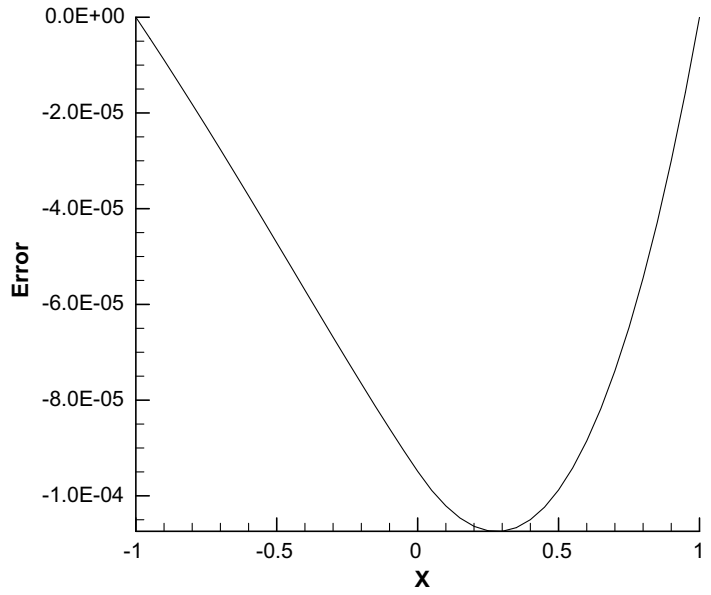

Fig. 17. Error distribution with $N = 40$, $l = 3$, finite difference method.

Table 1
Orders of different schemes for the 1D case

Order of jump condition	3-Point central difference	Chebyshev spectral	
		Collocation	Tau
1	1.50	1.45	2.11
2	2.00	1.99	3.14
3	2.00	3.90	4.21

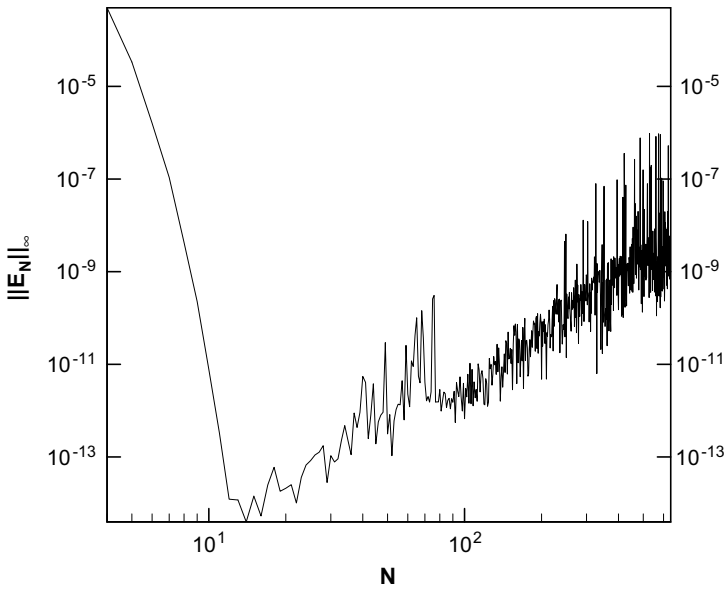

Fig. 18. Error of the Chebyshev collocation method for the 1D example with infinite order jump conditions.

$$(\widehat{\mathbf{D}}^{(2)} - \widehat{\mathbf{D}}^{(1)})\widehat{\mathbf{U}} = \widehat{\mathbf{P}}^{(1)} - \widehat{\mathbf{P}}^{(2)} \tag{35}$$

with $\widehat{\mathbf{U}} = (\hat{u}_0, \hat{u}_1, \ldots, \hat{u}_N)^{\mathbf{T}}$ as the unknown vector. The matrices $\widehat{\mathbf{D}}^{(2)}, \widehat{\mathbf{D}}^{(1)}$ and the vectors $\widehat{\mathbf{P}}^{(1)}$, $\widehat{\mathbf{P}}^{(2)}$ are defined by (18) and (19), respectively. The last two rows of (35) are replaced to represent the boundary condition, the same with classical tau method.

The decrease of the maximum error $\|E_N\|_\infty$ with the increase of N is illustrated in Figs. 19–22 with jump condition order l varies from 1 to 3 and $l = \infty$. It can be noticed that the oscillations of $\|E_N\|_\infty$ observed in finite difference and Chebyshev collocation schemes are greatly suppressed even at low order jump condition, and the scheme recovers the exponential convergence rate with infinite order jump condition in Fig. 22 (due to the restriction of machine precision, the maximum error $\|E_N\|_\infty$ does not continually reduce at $N > 14$). Comparisons between numerical results at $N = 40$ and the exact solution are shown in Figs. 23–26, and Figs. 27–30 give the spatial distribution of error at $N = 40$, $l = 1 \sim 3$ and $N = 10$, $l = \infty$. The orders of Chebyshev-tau method for this problem with different jump condition orders are calculated and shown in Table 1.

3. Higher dimensional cases

Extending (4) to higher dimension gives

$$u(\vec{x}) = u_c(\vec{x}) + \sum_{j=1}^{m} H(f_j) p_j(\vec{x}) \tag{36}$$

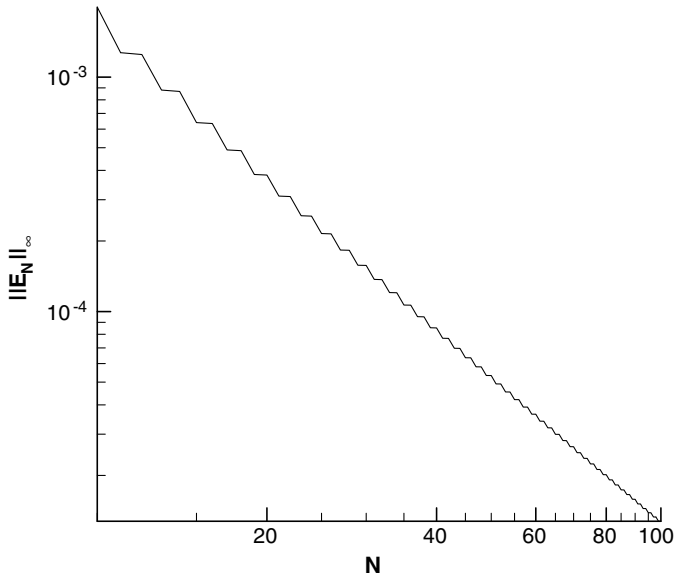

Fig. 19. Error of the Chebyshev-tau method for the 1D example with 1st order jump condition.

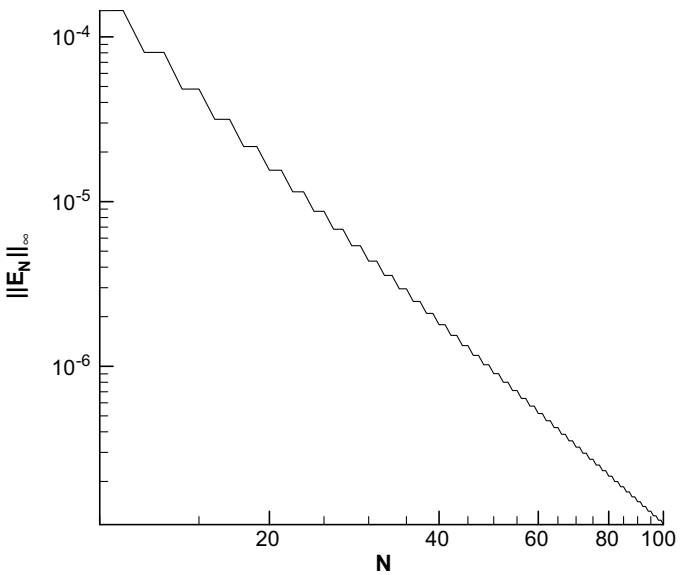

Fig. 20. Error of the Chebyshev-tau method for the 1D example with 2nd order jump condition.

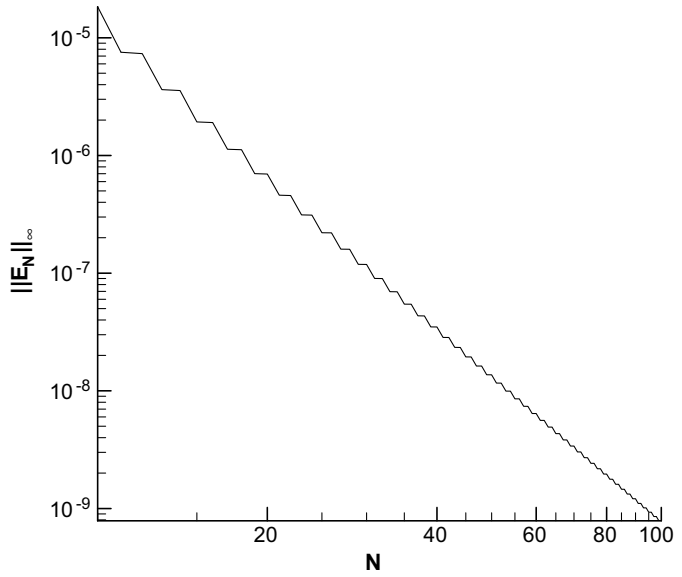

Fig. 21. Error of the Chebyshev-tau method for the 1D example with 3rd order jump condition.

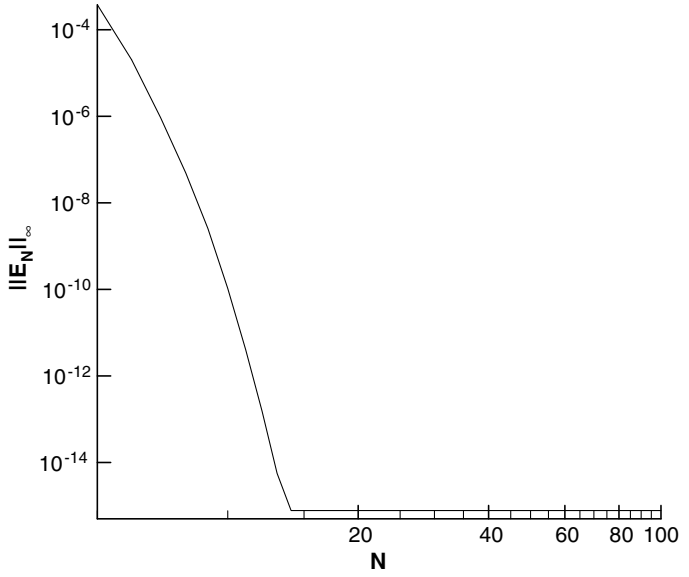

Fig. 22. Error of the Chebyshev-tau method for the 1D example with infinite order jump condition.

where $f_j = 0$ represents each discontinuous curve. Thus, it is possible to follow the one-dimensional cases and derive a high-dimensional version. Another treatment for the discontinuous curves chosen in the current paper is a dimension-by-dimension manner similar to [23]. More precisely, the derivative $\frac{\partial^n u}{\partial x_i^n}$ at point A is approximated using the values of discrete points along the line passing point A and parallel to x_i axis, which has discontinuous points on condition that it intersects one or more of the discontinuous curves $f_j = 0$. As an example, we consider a two-dimensional Poisson equation with a singular source, which is also used by LeVeque and Li [20], and Zhong [23]. The partial differential equation is

$$u_{xx} + u_{yy} = \int_\Gamma 2\delta(x - X(s))\delta(y - Y(s))\mathrm{d}s \quad \text{on} \quad \Omega = [-1, 1] \times [-1, 1] \tag{37}$$

where Γ is the circle $x^2 + y^2 = \frac{1}{4}$. Dirichlet boundary condition is given according to the exact solution

$$u = \begin{cases} 1 & \text{if} \quad r \leqslant 1/2 \\ 1 + \ln(2r) & \text{if} \quad r > 1/2 \end{cases} \tag{38}$$

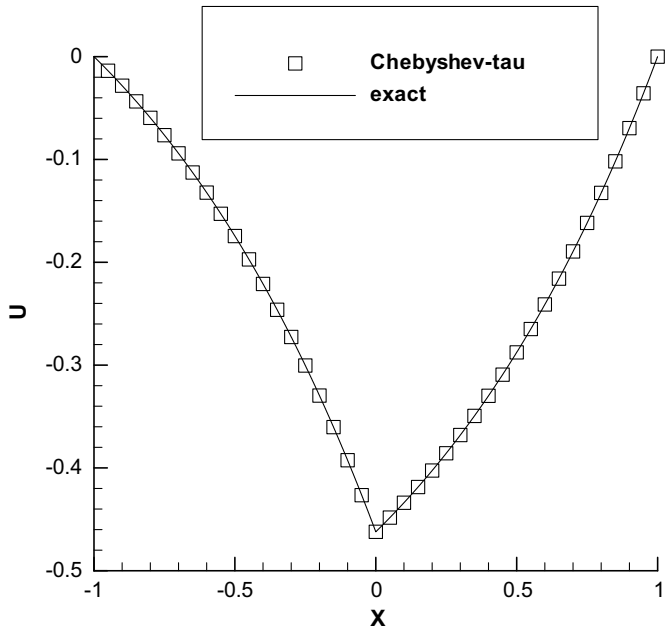

Fig. 23. Numerical solution for the 1D example using Chebyshev-tau method with $N = 40$, $l = 1$.

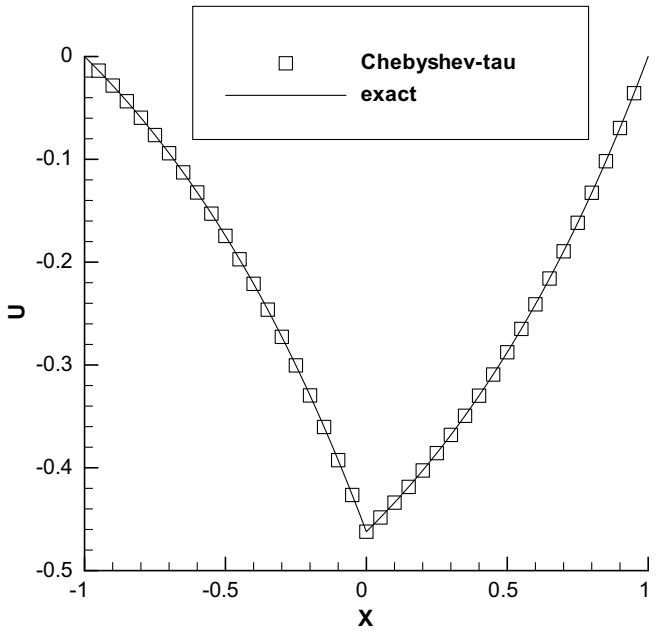

Fig. 24. Numerical solution for the 1D example using Chebyshev-tau method with $N = 40$, $l = 2$.

where $r = \sqrt{x^2 + y^2}$. Fig. 31 shows the plot of the exact solution (38). It is derived from the differential equation that $[u]|_\Gamma = 0$ and $[\partial u/\partial n]|_\Gamma = 2$.

In the following sections, we use the dimension-by-dimension approach to construct the finite difference and Chebyshev collocation schemes, and directly use (36) to construct a Chebyshev-tau scheme.

3.1. Finite difference and spectral collocation schemes

We denote the matrix $\mathbf{U}$ with its entries $u_{i,j}$ representing the approximation of exact solution u at point (x_i, y_j) and matrix $\mathbf{P}_{\mathbf{x}}^{(\mathbf{n})}$ with its jth column vector constructed by jump conditions along the line $y = y_j$. More detailedly, we denote the entries of

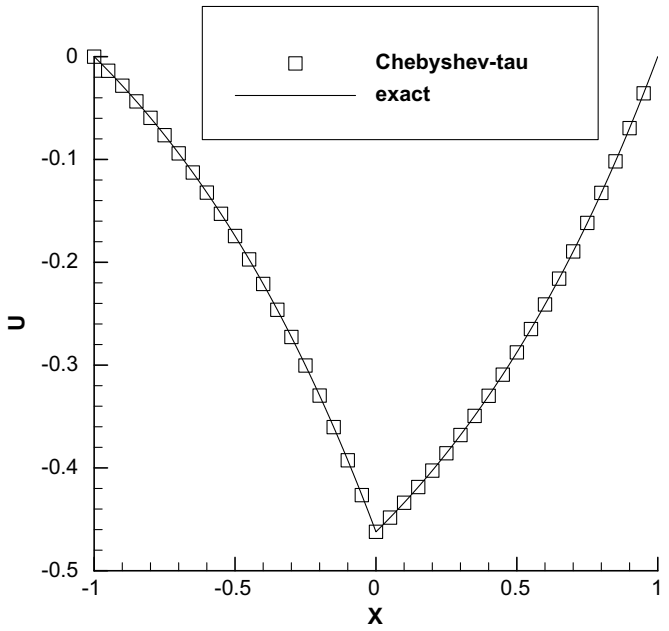

Fig. 25. Numerical solution for the 1D example using Chebyshev-tau method with $N = 40$, $l = 3$.

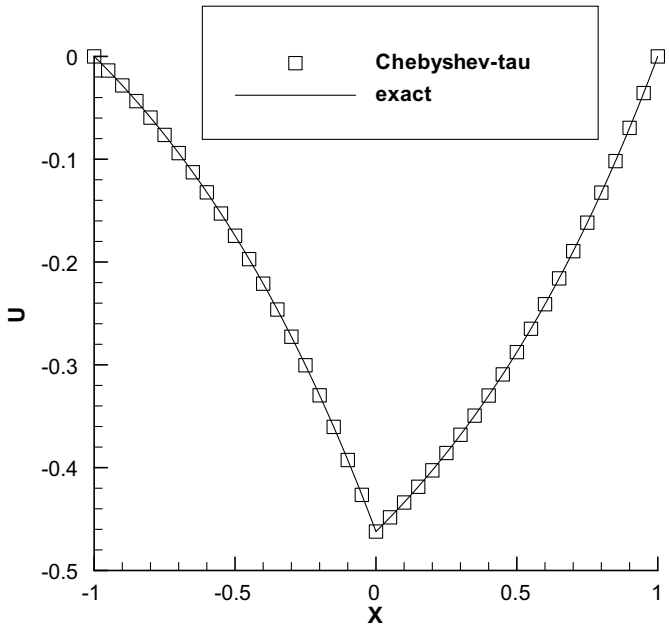

Fig. 26. Numerical solution for the 1D example using Chebyshev-tau method with $N = 40$, $l = \infty$.

$\mathbf{P}_{\mathbf{x}}^{(\mathbf{n})}$ as $p_{x,ij}^{(n)}$ and then consider an equivalent one-dimensional problem along the line $y = y_j$ with discontinuous points $x = \alpha_k$ being the intersections of the line $y = y_j$ and the interface Γ. Since the jump conditions $[u^{(n)}]|_{\alpha_k}$ are explicitly known beforehand, the corresponding correction functions $p_k^{(n)}(x)$ can be formed either using (22) or any other forms. Thus the corresponding jth column vector is constructed as

$$p_{x,ij}^{(n)} = \sum_k \left\{ H(x_i - \alpha_k) p_k^{(n)}(x_i) \right\} \tag{39}$$

As the extension of one-dimensional formula (12), it is easy to obtain that

$$\mathbf{U_{xx}} = \mathbf{D_{xx}U} - \mathbf{D_{xx}P_x} + \mathbf{P_x^{(2)}} \tag{40}$$

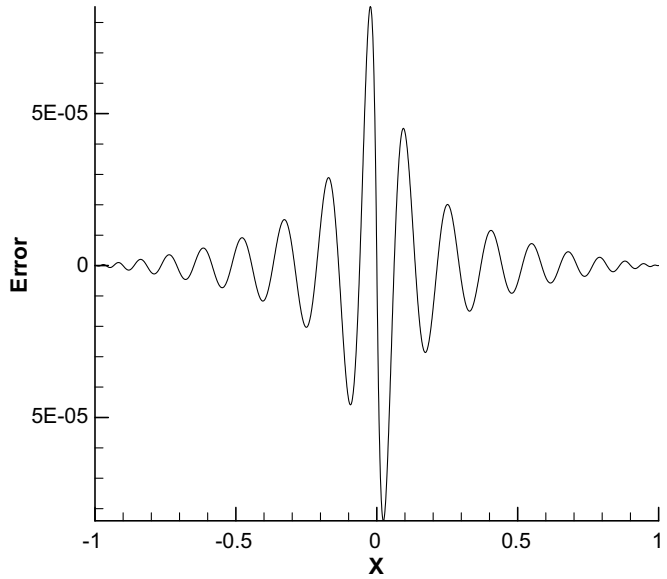

Fig. 27. Error distribution with $N = 40$, $l = 1$, Chebyshev-tau method.

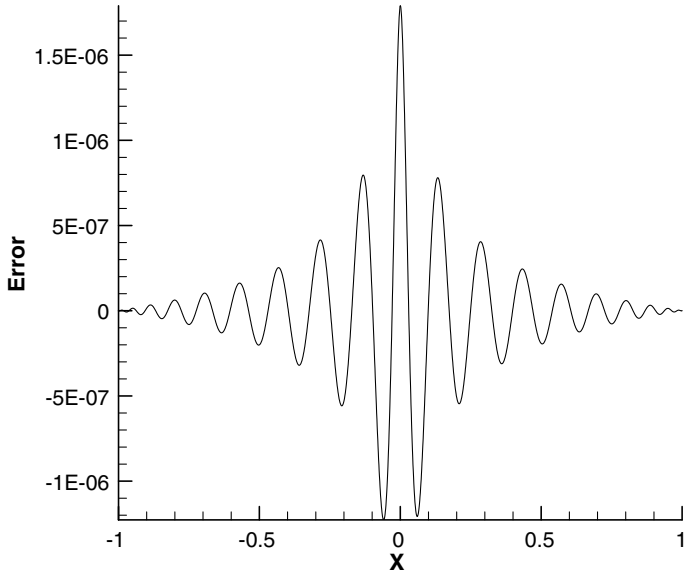

Fig. 28. Error distribution with $N = 40$, $l = 2$, Chebyshev-tau method.

Similarly, the y-direction derivative is approximated as

$$\mathbf{U_{yy}} = \mathbf{U}\mathbf{D}_{\mathbf{yy}}^{\mathbf{T}} - \mathbf{P_y}\mathbf{D}_{\mathbf{yy}}^{\mathbf{T}} + \mathbf{P}_{\mathbf{y}}^{(\mathbf{2})} \tag{41}$$

with the ith row vector of the matrix $\mathbf{P}_{\mathbf{y}}^{(\mathbf{n})}$ representing the jump conditions along the line $x = x_i$ and the superscript "**T**" denoting the transposition of a matrix. Thus the differential Eq. (37) is discretized as

$$\mathbf{D_{xx}}\mathbf{U} + \mathbf{U}\mathbf{D}_{\mathbf{yy}}^{\mathbf{T}} = \mathbf{D_{xx}}\mathbf{P_x} - \mathbf{P}_{\mathbf{x}}^{(\mathbf{2})} + \mathbf{P_y}\mathbf{D}_{\mathbf{yy}}^{\mathbf{T}} - \mathbf{P}_{\mathbf{y}}^{(\mathbf{2})} \tag{42}$$

The linear system (42) can be solved by a matrix diagonalization procedure described in [3].

Numerical simulations were carried out using 3-point (in each direction) central different and the Chebyshev collocation methods with an $N \times N$ grid at uniform points and Gauss-Lobatto points, respectively. Again, the accuracy is judged by the maximum error over all grid points

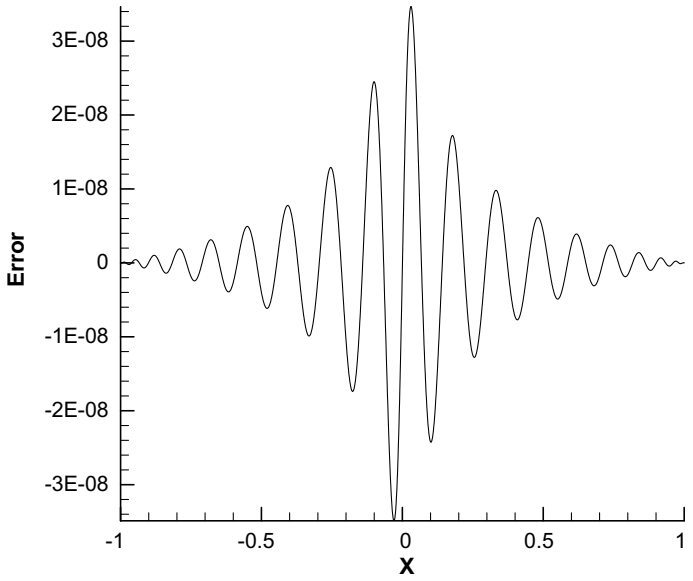

Fig. 29. Error distribution with $N = 40$, $l = 3$, Chebyshev-tau method.

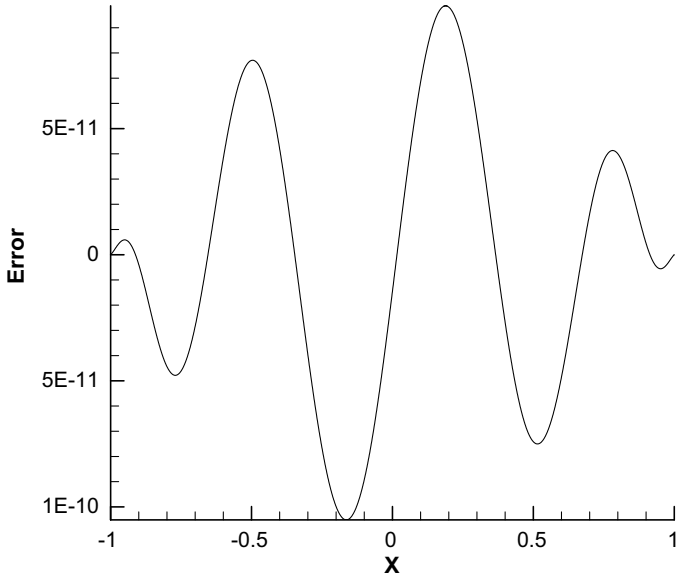

Fig. 30. Error distribution with $N = 40$, $l = \infty$, Chebyshev-tau method.

$$\|E_N\|_\infty = \max_{i,j} |u(x_i, y_j) - u_{i,j}| \tag{43}$$

and the definition of order r is the same with the one-dimensional case (32). Figs. 32 and 33 show the calculated $\|E_N\|_\infty$ at different grid densities. Numerical solution from Chebyshev collocation method is given in Fig. 34, and Fig. 35 shows a slice from Fig. 34 at $x = 0$. As shown in these figures, the sharp interface is successfully captured and there is no evidence of Gibbs oscillations.

In order to examine the convergence behavior, we gave the jump conditions for the 2nd order derivatives and compared the numerical results, with other computation configurations remaining unchanged. For the sake of simplicity, the jump conditions for the 2nd order derivatives were obtained directly from the exact solution. The calculated errors are shown in Figs. 36 and 37 for the finite difference method and the Chebyshev collocation method, respectively.

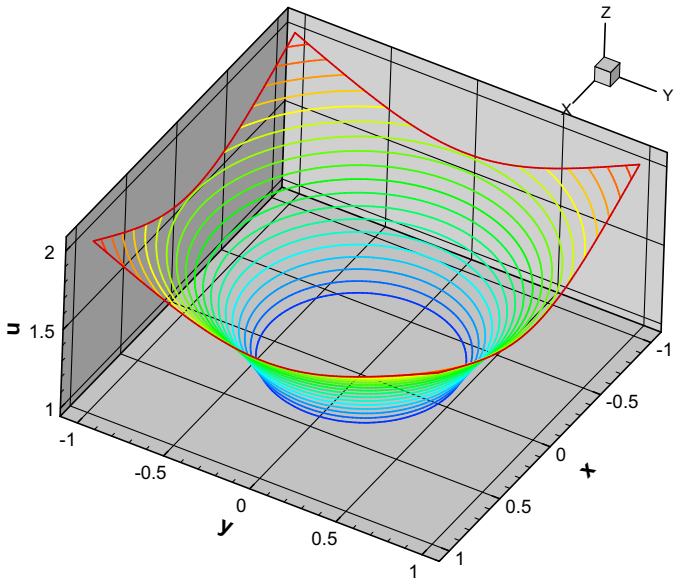

Fig. 31. Exact solution of the 2D example (37).

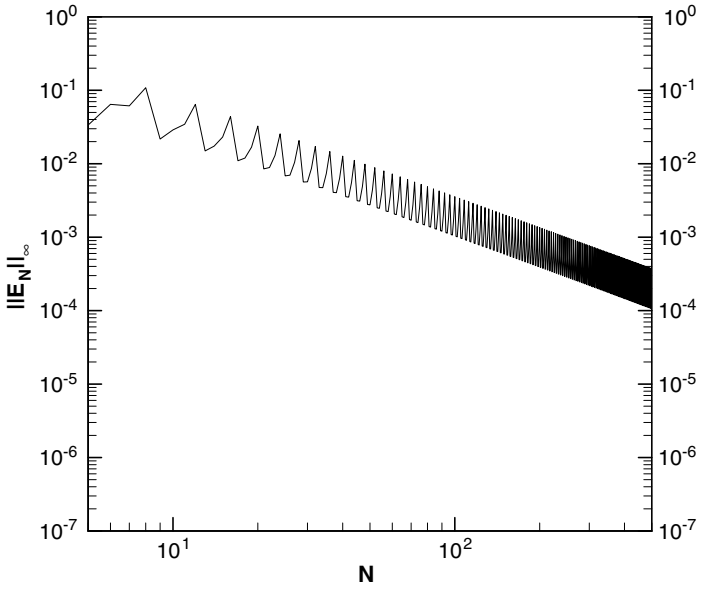

Fig. 32. Error of finite difference method for the 2D example with 1st order jump condition.

The comparison of orders of different schemes with different jump conditions is shown in Table 2. We also give a comparison between our present results and those by other authors (LeVeque and Li [20], Zhong [23]) in Table 3. It is seen from above comparison that present schemes provide acceptable accuracy for discontinuous problems. The satisfaction of higher order (second-order and above) jump conditions is apparently expected to bring an enhancement of the order of accuracy as well as a significant damp of the error oscillation. As shown in literature, it is possible to obtain higher order jump conditions either theoretically [21] or numerically [36].

3.2. Chebyshev-tau scheme

The 1st order jump condition of the differential Eq. (37) can be satisfied in the form of (36) by setting $f = \frac{1}{2} - r = \frac{1}{2} - \sqrt{x^2 + y^2}$ and $p(x, y) = -2r^2 + 1/2$, i.e. the solution of (37) was expanded in Chebyshev series as

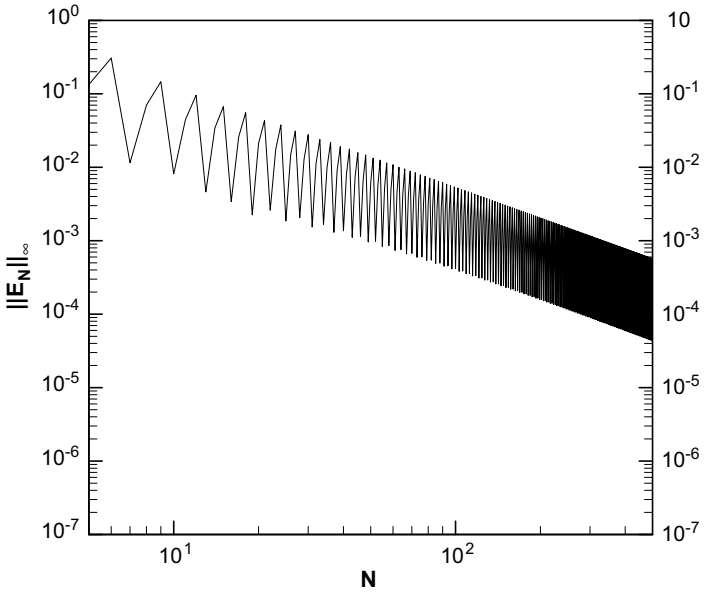

Fig. 33. Error of the Chebyshev collocation method for the 2D example with 1st order jump condition.

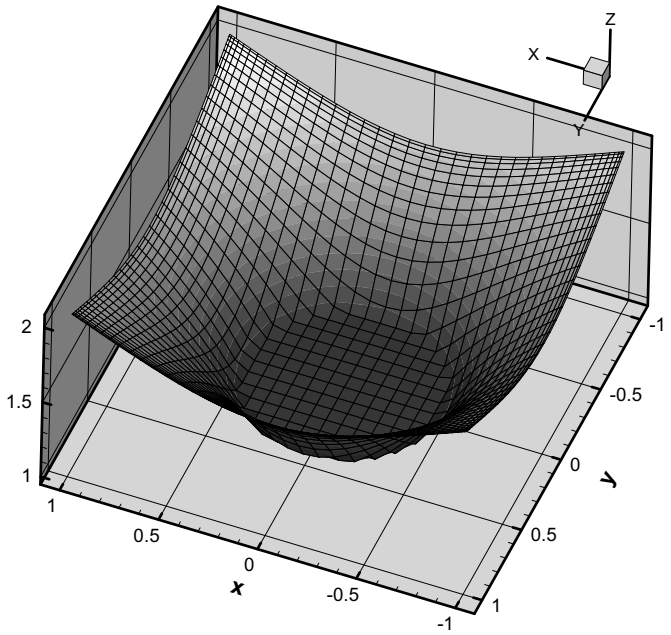

Fig. 34. Numerical solution of the 2D example with $N = 40$, $l = 1$, Chebyshev collocation method.

$$u = H\left(\frac{1}{2} - \sqrt{x^2 + y^2}\right)\left(-2x^2 - 2y^2 + \frac{1}{2}\right) + \sum_{i=0}^{N}\sum_{j=0}^{N}\hat{u}_{ij}T_i(x)T_j(y) \tag{44}$$

After substituting (44) into (37) and then applying the Galerkin weighted residual method, a linear system is acquired as

$$(\widehat{\mathbf{D}}^{(2)}\widehat{\mathbf{U}} + \widehat{\mathbf{U}}\widehat{\mathbf{D}}^{(2)})_{ij} = -\frac{4}{\pi^2 c_i c_j}\left[\int_S T_i(x)T_j(y)\frac{\partial^2 p}{\partial x^2}w(x)w(y)\mathrm{d}x\mathrm{d}y + \int_S T_i(x)T_j(y)\frac{\partial^2 p}{\partial y^2}w(x)w(y)\mathrm{d}x\mathrm{d}y\right] \tag{45}$$

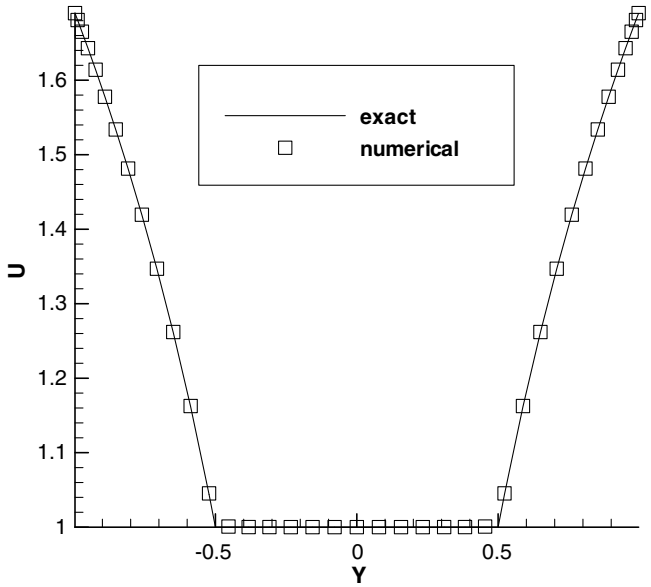

Fig. 35. Comparison between exact solution and numerical solution at line $x = 0$ with $N = 40$, $l = 1$, Chebyshev collocation method.

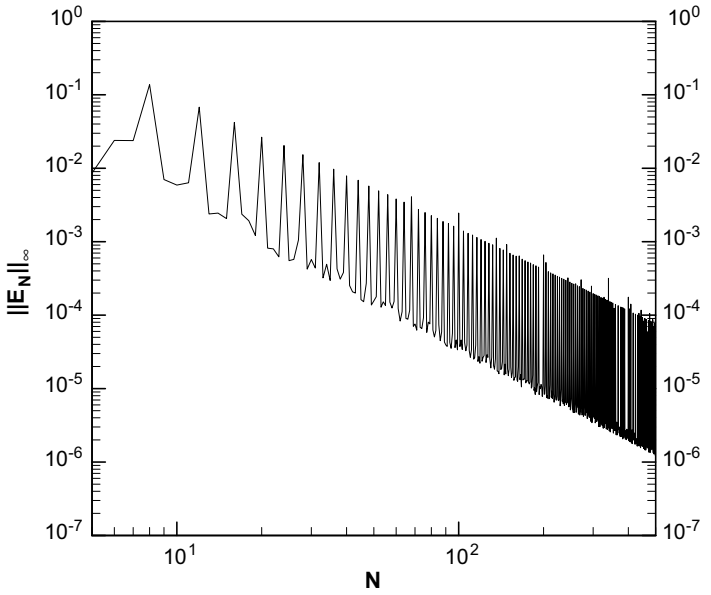

Fig. 36. Error of finite difference method for the 2D example with 2nd order jump condition.

where $\widehat{\mathbf{U}}$ is the unknown matrix with its entries being $\hat{u}_{ij}$ in (44), $w(t) = (1 - t^2)^{-1/2}$ is the weight function for Chebyshev spectral methods, c_k is the integration constant referred in (15) and S denotes the domain of integration

$$S = \left\{(x, y)|x^2 + y^2 < \frac{1}{4}\right\}$$

A matrix diagonalization procedure to solve the linear system (45) is also provided in [3].

Similarly, the 2nd order jump condition for this example can be satisfied by the selection of f and $p(x, y)$ in (36) that

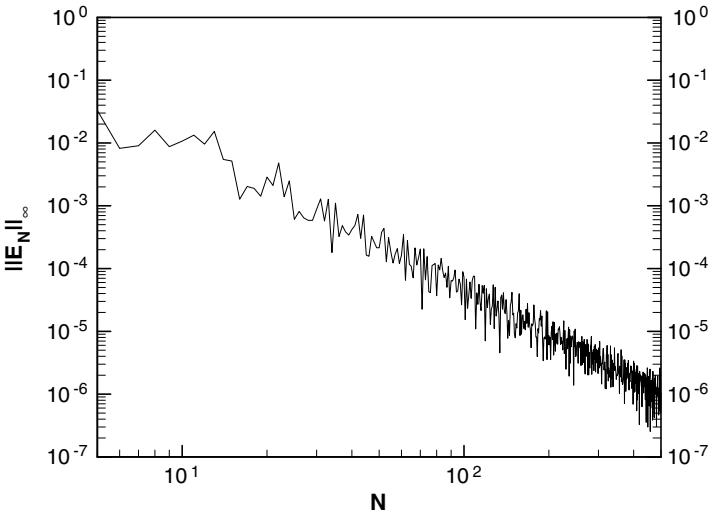

Fig. 37. Error of the Chebyshev collocation method for the 2D example with 2nd order jump condition.

Table 2
Orders of different schemes for the 2D case

Order of jump condition	Central difference	Chebyshev spectral	
		Collocation	Tau
1	1.38	1.36	2.44
2	2.06	2.36	3.61

Table 3
Accuracy comparison of present schemes and some other schemes from literatures [20,23]

	40×40 Grid	80×80 Grid
Discrete δ function method [20]	2.6467×10^{-2}	1.3204×10^{-2}
LeVeque and Li [20]	8.3461×10^{-4}	2.4451×10^{-4}
Zhong's method A (2nd order) [23]	1.6339×10^{-3}	2.8581×10^{-4}
Zhong's method B (2nd order) [23]	4.4405×10^{-4}	9.5040×10^{-5}
Zhong's method C (2nd order) [23]	1.5715×10^{-3}	2.5039×10^{-4}
Zhong's method D (3rd order) [23]	4.9529×10^{-4}	4.7499×10^{-5}
Zhong's method E (4th order) [23]	1.2215×10^{-4}	6.1514×10^{-6}
Zhong's method F (4th order) [23]	1.5521×10^{-5}	3.4286×10^{-7}
Present FD (1st order jump condition)	1.2699×10^{-2}	4.8724×10^{-3}
Present collocation (1st order jump condition)	1.3622×10^{-3}	3.2460×10^{-3}
Present FD (2nd order jump condition)	7.8715×10^{-3}	2.2626×10^{-3}
Present collocation (2nd order jump condition)	4.1955×10^{-4}	3.6900×10^{-5}
Present tau (1st order jump condition)	4.9248×10^{-4}	1.1441×10^{-4}
Present tau (2nd order jump condition)	7.1999×10^{-5}	8.5957×10^{-6}

$$
\begin{aligned}
f &= \tfrac{1}{2} - r \\
&= \tfrac{1}{2} - \sqrt{x^2 + y^2} \\
p(x,y) &= 4r^4 - 4r^2 + 3/4 \\
&= 4(x^2 + y^2)^2 - 4(x^2 + y^2) + 3/4
\end{aligned}
$$

The error $\|E_N\|_\infty$ is shown in Figs. 38 and 39 as a function of N. The order of current Chebyshev-tau scheme for the 2D example and the comparison of accuracy can be found in Tables 2 and 3, respectively. It can be seen from the 1D and 2D examples that tau methods seem to provide a higher accuracy and a smoother curve of error.

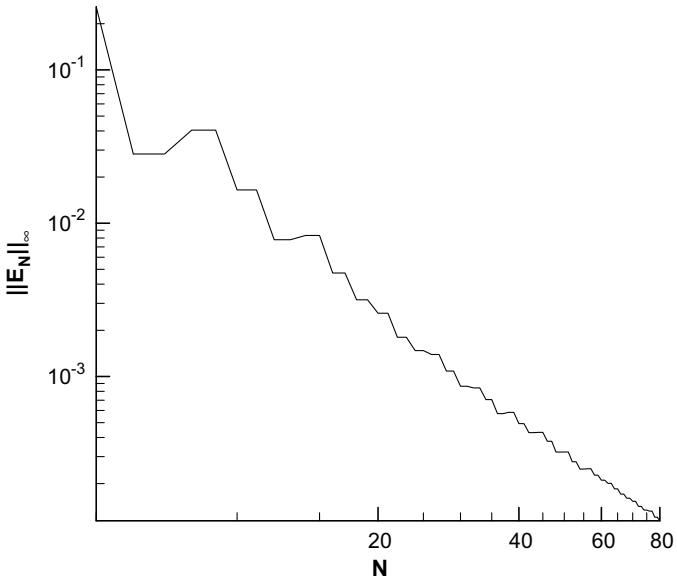

Fig. 38. Error of the Chebyshev-tau method for the 2D example with 1st order jump condition.

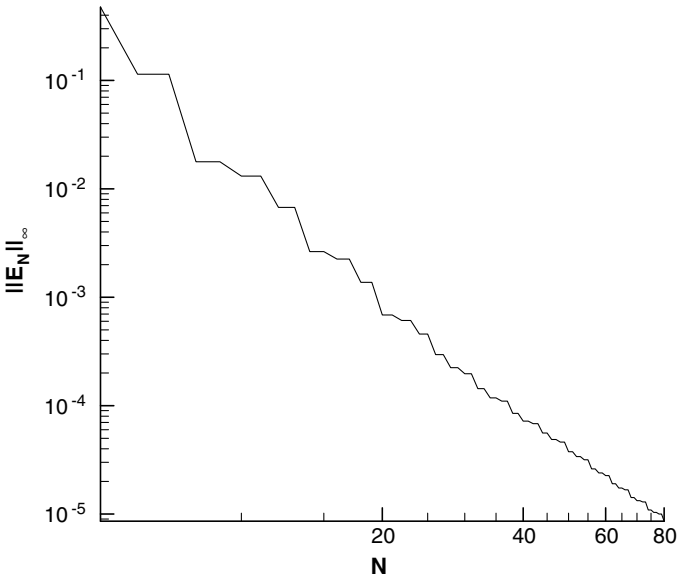

Fig. 39. Error of the Chebyshev-tau method for the 2D example with 2nd order jump condition.

4. Conclusions

A global description of discontinuous functions is proposed in this paper. By introducing the Heaviside function, a discontinuous function can be expressed as the sum of a smooth function and a correction term related to the jump conditions. This treatment enables us to use the spectral methods, which are originally developed for smooth problems, without incurring Gibbs phenomenon. Finite difference and other methods can also be combined with this concept. Only minor modifications are to be made to the original finite difference and spectral method and all correction terms are calculated explicitly. The order of finite difference and spectral methods we developed in this paper is limited by the number of available jump conditions. The accuracy of current Chebyshev collocation schemes are lower than those methods using special treatment near discontinuous points (e.g., [23,37]) but still comparable to LeVeque and Li's scheme [20]. However, Chebyshev-tau methods seem to have a higher accuracy. For some special cases where all jump conditions are known, our spectral methods can recover spectral accuracy.

The concept of global description proposes a new aspect to understand discontinuous functions and provides more flexibility in constructing schemes for discontinuous problems. Although the spectral methods proposed in the present paper do not reveal a significant accuracy improvement and the accuracy improvement may rely on higher order jump conditions (it is possible for some differential equations as evidenced in [21,36]), spectral methods may still be preferable for some other reasons even if the exponential convergence properties are diminished, for example, the ease of implementation in two or three dimensions and the advantages in handling certain boundary conditions (e.g., Fourier spectral methods for periodic boundary conditions) as mentioned in [40]. Besides, study on the convergence behavior of other schemes based on the current global description concept may also be valuable.

Acknowledgment

The sponsorships of the NSFC (Nos. 10472009, 50736007, 50136010) and Aviation Foundation (No. 05C51070) are acknowledged.

References

[1] C. Canuto, M.Y. Hussaini, A. Quarteroni, T.A. Zang, Spectral Methods in Fluid Dynamics, Springer Series in Computational Physics, Springer, New York, 1988.
[2] J.P. Boyd, Chebyshev and Fourier Spectral Methods, Dover, New York, 2000.
[3] R. Peyret, Spectral Methods for Incompressible Viscous Flow, Springer, New York, 2001.
[4] C.S. Peskin, Flow patterns around heart valves: a numerical method, J. Comput. Phys. 10 (1972) 220–252.
[5] D. Goldstein, R. Handler, L. Sirovich, Modeling a no-slip flow boundary with an external force field, J. Comput. Phys. 105 (1993) 354–366.
[6] M.-C. Lai, C.S. Peskin, An immersed boundary method with formal second-order accuracy and reduced numerical viscosity, J. Comput. Phys. 160 (2000) 705–719.
[7] B.E. Griffith, C.S. Peskin, On the order of accuracy of the immersed boundary method: higher order convergence rates for sufficiently smooth problems, J. Comput. Phys. 208 (2005) 75–105.
[8] R.P. Beyer, R.J. LeVeque, Analysis of a one-dimensional model for the immersed boundary method, SIAM J. Numer. Anal. 29 (1992) 332–364.
[9] A.K. Tornberg, B. Engquist, Numerical approximations of singular source terms in differential equations, J. Comput. Phys. 200 (2004) 462–488.
[10] B. Engquist, A.-K. Tornberg, R. Tsai, Discretization of Dirac delta function in level set methods, J. Comput. Phys. 207 (2005) 28–51.
[11] E.M. Saiki, S. Biringen, Numerical simulation of a cylinder in uniform flow: application of a virtual boundary method, J. Comput. Phys. 123 (1996) 450–465.
[12] P.N. Watton, X.Y. Luo, et al., Dynamic modelling of prosthetic chorded mitral valves using the immersed boundary method, J. Biomech. 40 (2007) 613–626.
[13] L.J. Fauci, C.S. Peskin, A computational model of aquatic animal locomotion, J. Comput. Phys. 77 (1988) 85–108.
[14] L.J. Fauci, Interaction of oscillating filaments: a computational study, J. Comput. Phys. 86 (1990) 294–313.
[15] A.L. Fogelson, C.S. Peskin, A fast numerical method for solving the three-dimensional Stokes' equations in the presence of suspended particles, J. Comput. Phys. 79 (1988) 50–69.
[16] D. Sulsky, J.U. Brackbill, A numerical method for suspension flow, J. Comput. Phys. 96 (1991) 339–368.
[17] E.A. Fadlun, R. Verzicco, et al., Combined immersed-boundary finite-difference methods for three-dimensional complex flow simulations, J. Comput. Phys. 161 (2000) 35–60.
[18] E. Jung, C.S. Peskin, Two-dimensional simulations of valveless pumping using the immersed boundary method, SIAM J. Sci. Comput. 23 (2001) 19–45.
[19] E. Balaras, Modeling complex boundaries using an external force field on fixed Cartesian grids in large-eddy simulations, Comput. Fluids 33 (2004) 375–404.
[20] R.J. LeVeque, Z. Li, The immersed interface method for elliptic equations with discontinuous coefficients and singular sources, SIAM J. Numer. Anal. 31 (1994) 1019–1044.
[21] S. Xu, Z.J. Wang, Systematic derivation of jump conditions for the immersed interface method in three-dimensional flow simulation, SIAM J. Sci. Comput. 27 (2006) 1948–1980.
[22] S. Xu, Z.J. Wang, An immersed interface method for simulating the interaction of a fluid with moving boundaries, J. Comput. Phys. 216 (2006) 454–493.
[23] X. Zhong, A new high-order immersed interface method for solving elliptic equations with imbedded interface of discontinuity, J. Comput. Phys. 225 (2007) 1066–1099.
[24] Z. Li, An overview of the immersed interface method and its applications, Taiwan. J. Math. 7 (2003) 1–49.
[25] L. Adams, Z.L. Li, The immersed interface/multigrid methods for interface problems, SIAM J. Sci. Comput. 24 (2002) 463–479.
[26] L. Adams, T.P. Chartier, New geometric immersed interface multigrid solvers, SIAM J. Sci. Comput. 25 (2004) 1516–1533.
[27] P.A. Berthelsen, A decomposed immersed interface method for variable coefficient elliptic equations with non-smooth and discontinuous solutions, J. Comput. Phys. 197 (2004) 364–386.
[28] W.-C. Wang, A jump condition capturing finite difference scheme for elliptic interface problems, SIAM J. Sci. Comput. 25 (2004) 1479–1496.
[29] A. Wiegmann, K.P. Bube, The explicit-jump immersed interface method: finite difference methods for PDEs with piecewise smooth solutions, SIAM J. Numer. Anal. 37 (2000) 827–862.
[30] Z.L. Li, The immersed interface method using a finite element formulation, Appl. Numer. Math. 27 (1998) 253–267.
[31] L. Lee, R.J. LeVeque, An immersed interface method for incompressible Navier–Stokes equations, SIAM J. Sci. Comput. 25 (2003) 832–856.
[32] G.H. Cottet, B. Michaux, et al., A comparison of spectral and vortex methods in three-dimensional incompressible flows, J. Comput. Phys. 175 (2002) 702–712.
[33] A. Meseguer, L.N. Trefethen, Linearized pipe flow to Reynolds number 10^7, J. Comput. Phys. 186 (2003) 178–197.
[34] J. Leypoldt, H.C. Kuhlmann, H.J. Rath, Three-dimensional numerical simulation of thermocapillary flows in cylindrical liquid bridges, J. Fluid Mech. 414 (2000) 285–314.
[35] K. Bergeron, E.A. Coutsias, J.P. Lynov, A.H. Nielsen, Dynamical properties of forced shear layers in an annular geometry, J. Fluid Mech. 402 (2000) 255–289.
[36] M.N. Linnick, F.F. Hermann, A high-order immersed interface method for simulating unsteady incompressible flows on irregular domains, J. Comput. Phys. 204 (2004) 157–192.
[37] Y.C. Zhou, S. Zhao, M. Feig, G.W. Wei, High order matched interface and boundary method for elliptic equations with discontinuous coefficients and singular sources, J. Comput. Phys. 213 (2006) 1–30.
[38] K.M. Arthurs, L.C. Moore, C.S. Peskin, E.B. Pitman, H.E. Layton, Modeling arteriolar flow and mass transport using the immersed boundary method, J. Comput. Phys. 147 (1998) 402–440.

[39] N.K.R. Kevlahan, J.-M. Ghidaglia, Computation of turbulent flow past an array of cylinders using a spectral method with Brinkman penalization, Eur. J. Mech. – B/Fluids 20 (2001) 333–350.
[40] K. Schneider, Numerical simulation of the transient flow behaviour in chemical reactors using a penalisation method, Comput. Fluid. 34 (2005) 1223–1238.
[41] G.H. Keetels, U. D'Ortona, W. Kramer, H.J.H. Clercx, K. Schneider, G.J.F. van Heijst, Fourier spectral and wavelet solvers for the incompressible Navier–Stokes equations with volume-penalization: convergence of a dipole-wall collision, J. Comput. Phys. (2007), doi:10.1016/j.jcp.2007.07.036.
[42] S. Abarbanel, D. Gottlieb, E. Tadmor, Spectral methods for discontinuous problems, in: K.W. Morton, M.J. Baines (Eds.), Numerical Methods for Fluid Dynamics II, Clarendon Press, 1986, pp. 129–153.